Structural and electronic properties of protein/thiolate-protected gold nanocluster with "staple" motif: A XAS, L-DOS, and XPS study

Gordon A. Simms, J. Daniel Padmos, and Peng Zhang

Citation: The Journal of Chemical Physics **131**, 214703 (2009); doi: 10.1063/1.3268782
View online: http://dx.doi.org/10.1063/1.3268782
View Table of Contents: http://scitation.aip.org/content/aip/journal/jcp/131/21?ver=pdfcov
Published by the AIP Publishing

Structural and electronic properties of protein/thiolate-protected gold nanocluster with "staple" motif: A XAS, L-DOS, and XPS study

Gordon A. Simms, J. Daniel Padmos, and Peng Zhang[a)]
Department of Chemistry and Institute for Research in Materials, Dalhousie University, Halifax, Nova Scotia B3H 4J3, Canada

(Received 3 October 2009; accepted 4 November 2009; published online 3 December 2009)

Following the recent breakthrough of total structural determination of a Au-thiolate nanocluster [P. Jadzinsky *et al.*, Science **318**, 430 (2007)], extensive interests have been stimulated to unveil (or revisit) the structure-property relationship of various thiolate-Au nanostructures in light of the new finding of $-SR-(Au-SR)_x-$ "staple" motif. Here, we present experimental x-ray absorption spectroscopy (XAS) and x-ray photoelectron spectroscopy (XPS) results on the local structure and electronic properties of thiolate-protected Au nanocluster encapsulated in bovine serum albumin (Au-BSA) together with theoretical calculation of projected local density of states (l-DOS) of $Au_{25}(SR)_{18}$ model cluster. Analysis of the Au L_3-edge extended x-ray absorption fine structure (EXAFS) of Au-BSA suggested that the nanocluster is Au_{25} with Au-thiolate "staple" motif. X-ray absorption near-edge structure (XANES) and Au 4f XPS were used to probe the electronic behavior of Au-BSA. The Au d-electron density of Au-BSA was found to decrease by 0.047 e^- relative to that of the bulk. A self-consistent real space Green's function approach implemented in *ab initio* FEFF8 program was used to calculate the l-DOS of $Au_{25}(SR)_{18}$ and other model clusters from a site-specific perspective. The theoretical results are in good agreement with the experimental d-DOS data of Au-BSA and, importantly, systematically illustrate the effect of Au-thiolate "staple" motif on the electronic behavior of $Au_{25}(SR)_{18}$. The present work sheds light on the structure-property relationship of thiolate-protected Au_{25} from both experimental and theoretical perspectives and illustrates the usefulness of XAS/l-DOS method in such studies. © *2009 American Institute of Physics*. [doi:10.1063/1.3268782]

I. INTRODUCTION

The recent breakthrough[1] of total structural determination of Au-thiolate nanocluster (NC) $Au_{102}(SR)_{44}$ has stimulated extensive interests in the synthesis and structure-property studies of various thiolate-Au nanostructures in light of the discovery of Au-thiolate "staple" motif.[2–7] The "staple" motif can be described as Au-thiolate moieties in the form of $-SR-(Au-SR)_x-$ (x=1 or 2), which cap the surface of a "grand" Au core like a staple (when x=1). Theoretical studies[8] have been quite successful in interpreting and/or predicting the atomic structure and properties of thiolate-protected NCs such as Au_{25},[4] Au_{38},[9] Au_{102},[10] and Au_{144}.[11] Undoubtedly, previous [prior to the structural determination of $Au_{102}(SR)_{44}$] and recent achievements in Au-thiolate NC synthesis play a crucial role in the research progress in this area.[5,12–15] It is noteworthy that not only small thiol ligands, but large sulfur-rich proteins such as bovine serum album (BSA) can be used to prepare thiolate-protected NCs. Ying *et al.*[16] recently reported the synthesis of BSA-encapsulated Au_{25} which showed greatly enhanced luminescence intensity, making them promising candidates for biotechnological applications. Despite of these progresses, what remains challenging[17] is how to systematically understand the relationship between the atomic structure (particularly related to the "staple" motif) and the physiochemical properties of these NCs. Toward this end, new results on the characterization of Au_{25} NCs using mass spectrometry,[18] femtosecond laser spectroscopy,[19] electrochemistry,[15] and NMR techniques[20] have provided useful insights into the structure and properties of the Au NCs.

X-ray absorption spectroscopy (XAS), including both extended x-ray absorption fine structure (EXAFS) and x-ray absorption near-edge structure (XANES), have been demonstrated very useful in illustrating the local structure (EXAFS) and electronic property (XANES) of NCs.[21–23] Joint use of EXAFS and XANES, particularly when in association with theoretical simulations, has been used to provide detailed information about the local structure and electronic behavior of NCs with various morphology, composition and surface chemistry.[24,25] Recent development of theoretical XAS codes such as FEFF8 program further empowers the experimental XAS by self-consistent calculations of projected local density of states (l-DOS).[26] In the context of electronic study of transition metal NCs, x-ray photoelectron spectroscopy (XPS) has also been extensively used.[23,27–29] The joint use of XAS and XPS, which are complimentary in electronic transition process, was very useful in providing a more complete physical picture of the electronic properties.[23] Herein, we report an experimental study (EXAFS, XANES, and XPS) of Au-BSA together with theoretical l-DOS calculation of $Au_{25}SR_{18}$ model cluster. The EXAFS suggested a structure

a)Author to whom correspondence should be addressed. Electronic mail: peng.zhang@dal.ca.

of Au_{25} with Au-thiolate "staple" motif for Au-BSA. The electronic behavior of the protein-encapsulated Au NCs was investigated with XANES and XPS and the experimental findings were compared with the theoretical l-DOS results from a site-specific perspective. What emerged from this work is a detailed picture of l-DOS behavior and unique structural/electronic properties of Au-thiolate NCs associated with the "staple" motif.

II. EXPERIMENTAL SECTION

A. Preparation of Au-BSA

All chemicals (of high purity) were purchased from Aldrich or Alfa Aesar and used without further purification. Ultrapure water (18.2 MΩ) was used in all experiments. Au-BSA was prepared according to the following procedure: 200 μl of a 30 mM $HAuCl_4$ solution was added to 10 ml of a 60 nM BSA solution. With stirring, the mixture was bubbled with argon for 10 min via a glass pipet. Next, 100 μl of a 30 mM $NaBH_4$ solution was added dropwise under vigorous stirring. This solution was then stirred for 1 h at room temperature. The resultant solution was stored in a fridge and used as-prepared for further characterization. It was found that the Au-BSA sample was very stable (no change of color and morphology for at least 6 months). Morphology of the NCs was characterized with a JEOL 123 transmission electron microscopy (TEM) operated at a voltage of 80 keV.

B. Synchrotron X-ray experiments

Synchrotron XPS experiments were conducted at the SGM beamline of the Canadian Light Source (CLS) operated at 2.9 GeV. The Au-BSA sample was mounted onto a silicon wafer for XPS measurement. X-ray excitation energies at 400, 500, and 700 eV were selected to collect Au 4f spectra. The XPS binding energies were calibrated using the carbon (285.00 eV) 1s peak. The Au L_3-edge XAS experiments were performed at the HXMA beamline of CLS using a transmission mode. The Au-BSA film was loaded onto an adhesive tape which was folded several times to achieve the best transmission signal. A simultaneous collection of the XAS data of Au foil was performed for each measurement to ensure a reliable measurement of the E_0 shift of the NCs relative to the bulk. The XAFS data were normalized and converted to k and R space with WINXAS program[30] using the standard procedure previously described.[25] A semiquantitative analysis of d-hole counts of the Au NCs was conducted following the method reported by Sham *et al.*[31] In Sham's method, d-hole counts of Pd and Ag alloy samples were calculated based on the scaling factor derived from the ratio of the area under the difference curve between the L_3-edge XANES of Pd and Ag metal to a difference hole count of 0.928. In this work, the same strategy was taken; Au and Pt foil references were used for the calculation of Au d-hole counts. The d-hole counts of bulk Au (0.631) and Pt (1.534) were obtained from our FEFF8 l-DOS calculation. The Au L-edge white line intensity was determined by integrating the XANES from −10 eV below to 7.5 eV above the E_0.

C. Theoretical studies

The l-DOS calculation was conducted using FEFF8 program.[26] The atomic coordinates of $Au_{25}S_{18}$ used in the FEFF input file was taken from literature.[32] The calculation was conducted both in the presence of a core hole and by completely screening the core hole using a NOHOLE (i.e., assuming a core hole is completely screened) card. Results on the change of d-electron counts calculated from these two methods were found to be similar. Because the NOHOLE approach gives better agreement for d-DOS and L-edge absorption calculations,[26] data presented in the discussion were taken from this approach.

The EXAFS fitting was performed using theoretical phase shift and amplitude generated by FEFF8 program. Structural model of bulk Au and Au_2S were used for fitting the first shell Au–Au and Au–S bonds. EXAFS signal $\chi(k)$ was extracted using WINXAS program based on the following equation:

$$\chi(k) = \frac{\mu(k) - \mu_0(k)}{\mu_0(k)},$$

where k is the photoelectron wavevector $[k = \sqrt{2m/\hbar^2(E-E_0)}]$, $\mu(k)$ the measured X-ray absorption coefficient, and $\mu_0(k)$ the isolated-atom background function.

The theoretical EXAFS signal $\chi(k)$ is normally expressed as

$$\chi(k) = \sum_j \frac{N_j S_0^2 F_j(k)}{kR_j^2} e^{(-2k^2\sigma^2)} e^{(-2R_j/\lambda)} \sin[2kR_j + \delta_j(k)]$$

Here $F(k)$ is the backscattering amplitude from each of the N_j neighboring atoms of the jth type with a Debye–Waller factor of σ_j which accounts for thermal vibration (assuming harmonic vibration) and static disorder (assuming Gaussian pair distribution) and at a distance R_j away. The quantity $\delta(k)$ is the total phase shift experienced by the photoelectron and S_0^2 is the amplitude reduction factor. When anharmonic contribution to the pair distribution function needs to be considered, the third cumulant (C_3) (Ref. 33) should be considered and the theoretical $\chi(k)$ is written as

$$\chi(k) = \sum_j \frac{N_j S_0^2 F_j(k)}{kR_j^2} e^{(-2k^2\sigma^2)} e^{(-2R_j/\lambda)} \times \sin\left[2kR_j + \delta_j(k) - \frac{4}{3}C_3 k^3\right]$$

Structural parameters from the experimental EXAFS data were then obtained by a nonlinear least-squares fit of the theoretical $\chi(k)$, which was conducted in R space by Fourier transforming $\chi(k)$.

III. RESULTS AND DISCUSSION

A. Structural analysis of Au-BSA

Figure 1 shows the TEM image of Au-BSA. It is seen that aggregates of BSA appear as dark gray background and the encapsulated NCs (small black dots) were observed in the same area.[34] Average size of the NCs was estimated to be ~1 nm. The TEM resolution was obscured by the envelop-

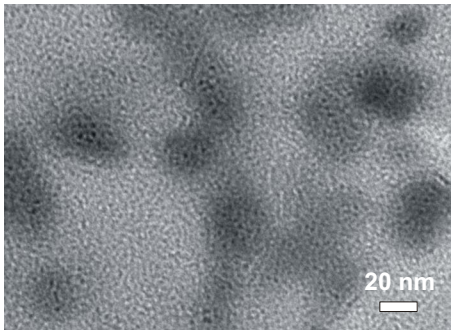

FIG. 1. A representative TEM image of BSA-encapsulated Au NCs. The Au NCs are seen in the image as small black dots.

ing protein and thus accurate size distribution data cannot be obtained.[34] Au L_3-edge EXAFS was then performed to provide more detailed structural information. Note that ideally sulfur-specific XAS (and XPS) may also provide useful structural information of the thiolate-Au NCs.[23] However, due to the presence of extra free sulfur atoms (not binding to gold) in BSA, x-ray data from sulfur-perspective will be much more complicated. Therefore, in the present work we only focus on the x-ray spectroscopy studies from Au perspective. Figure 2 displays the *k*-space and Fourier-transformed Au L_3-edge EXAFS (without phase correction) of Au-BSA and bulk Au. In the *k*-space spectra in Fig. 2(a), the EXAFS oscillatory pattern of Au-BSA is considerably different from that of the fcc bulk Au, which may be attributed to the presence of a large fraction of Au–S bonds and the absence of the fcc crystalline structure in a very small Au cluster. Moreover, the EXAFS intensity of Au-BSA is significantly lower than that of bulk Au. This is an indication of

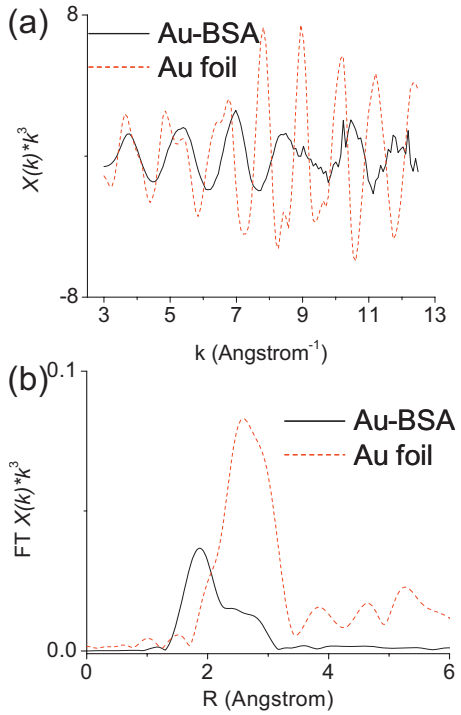

FIG. 2. Experimental EXAFS data of Au–BSA (solid line) and Au foil (dashed line) plotted in (a) k^3-space and (b) *R*-space (without phase correction).

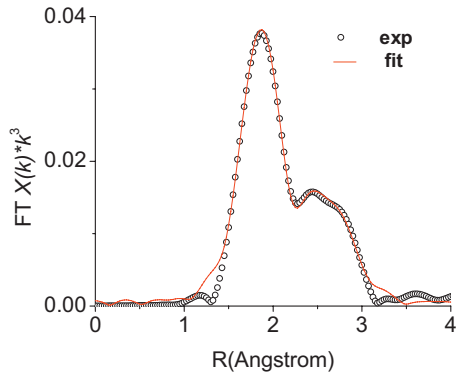

FIG. 3. Experimental FT-EXAFS (open circle) and the best fit (solid line). The fitting was done with a k range of 3–12 $Å^{-1}$ and selection of the first shell Au–S and Au–Au bonds (1.5–3.1 Å in FT-EXAFS).

a very small size of the NCs. In other words, the average coordination number (CN) of Au in the NCs is much lower than that of the bulk. In the FT-EXAFS in Fig. 2(b), two types of chemical bonds in the first shell, Au–S and Au–Au, are clearly seen.

In order to obtain quantitative structural information, nonlinear least-squares fit of the first shell FT-EXAFS was conducted. The theoretical scattering amplitudes and phase shifts of Au_2S and bulk Au calculated with FEFF8 were used, following the method by Menard *et al.*[33] The transferability of scattering amplitudes and phase shifts of bulk (Au_2S and Au) references in fitting the EXAFS of NCs was assumed in the analysis of Au-BSA. Such an assumption has worked well in the EXAFS analysis of thiolate-protected Au_{13} NCs.[33] The value (0.9) of amplitude reduction factor S_0^2 was determined from fitting the EXAFS of Au foil. *R*-range of 1.5–3.1 Å was chosen for the first shell fitting. The fit results are presented in Fig. 3 and Table I. The first shell CN and bond distance data of $Au_{25}(SR)_{18}$ reported by Murray *et al.*[3] and EXAFS fit results of bulk Au were also given in the table for comparison. The most striking findings in our EXAFS analysis are the CN data of Au-BSA, which give a first shell Au–S CN of 1.2 and a Au–Au CN of 3.0. The Au–S CN is unusually high relative to that of other thiolate-protected Au NCs reported in the literature [e.g., CN=0.8 for Au_{13} (Ref. 33)] and approaches to that of $(–Au–SR–)_n$ polymer (CN =2). In addition, the Au–Au CN of Au-BSA is only 3.0, much lower even than that of Au_{13}(CN=6.2) determined by EXAFS.[33] The unusually high Au–S and low Au–Au CN of Au-BSA can only be accounted for by the presence of Au-thiolate "staple" motif. Indeed, presence of the $–SR–(Au–SR)_x–$ (x=1 or 2) "staples" in the NCs can both increase the average Au–S CN (Au in the "staple" has two S neighbors) and decrease the average Au–Au CN (Au in the "staple" has zero Au neighbor). The fact that the CN values of Au-BSA is very close to the theoretical ones of $Au_{25}(SR)_{18}$ in Table I [$CN_{Au–S}$=1.4 and $CN_{Au–Au}$=3.3 for $Au_{25}(SR)_{18}$ versus $CN_{Au–S}$=1.2(1) and $CN_{Au–Au}$=3.0(4) for Au-BSA] suggests that the Au-BSA NCs prepared in this work are mostly likely Au_{25}. This notion is further supported by the finding of the much higher stability of Au_{25} than other thiolate-protected Au_n NCs with different numbers of Au atoms in the range of n=10–39.[35] It must be noted, however,

TABLE I. EXAFS fit results of Au-BSA and structural data of relevant references.

	Bonding	CN	R (Å)	σ^2	E_0 (eV)	C_3
$Au_{25}(SR)_{18}$	Au–S	1.4	2.32/2.38	⋯	⋯	⋯
	Au–Au	3.3	2.79/2.81/2.96	⋯	⋯	⋯
Au-BSA	Au–S	1.2(1)	2.30(1)	0.004(1)	−2.2(5)	⋯
	Au–Au	3.0(4)	2.81(1)	0.010(1)	0.8(2)	0.0012(2)
Au foil	Au–Au	12 (fixed)	2.86(1)	0.008(1)	1.0(5)	⋯

that there still exists a small difference between the CNs of Au-BSA and those of $Au_{25}(SR)_{18}$ model cluster. Such a difference is plausibly caused by the presence of a small amount of $Au_n(SR)_m$ where $n \neq 25$ and/or $m \neq 18$, whose stability was enhanced by the giant protein (BSA) protecting ligand. A comparison of the current data with the EXAFS of small ligand-protected $Au_{25}(SR)_{18}$ NCs would be useful to verify this hypothesis in the future. In addition, the uncertainty of EXAFS fitting results (e.g., $CN_{Au-Au}=3.0\pm0.4$) associated with the limited usable k-space data (3–12 $Å^{-1}$) may also contribute to the difference of the CNs. Burt *et al.*[34] studied the structure of a series of BSA-protected Au NCs with TEM. Although they did observe NCs of ~1 nm with high-resolution transmission electron microscopy, the average sizes (1.5–1.8 nm) obtained by their HAADF- scanning transmission electron microscopy measurements are larger than that of Au_{25} (0.98 nm according to Murray *et al.*[3]). We interpret this discrepancy as the difference of the synthetic conditions, which are sensitive in determining the yield of Au_{25} stabilized with either small ligands or proteins.[5,16]

The first shell Au–S bond distance (2.30 Å) from our EXAFS analysis is slightly shorter than that $Au_{25}(SR)_{18}$ reported by Murray *et al.*[3] (2.35 Å on average). This finding implied that the molecular structure of protecting ligands (small thiolate versus BSA) can influence the structure of Au-thiolate "staples." Indeed, BSA can be considered as a single giant protecting ligand (molecular weight 66 k Dalton) with 35 thiol-bearing cysteine residues.[34] The unique tertiary structure of BSA naturally play a special role in determining the geometry of Au-thiolate "staples" of the NCs, which were encapsulated in the protein matrix. The Au–Au bond distance of Au-BSA (2.81 Å) is considerably shorter than that of Au foil reference (2.86 Å) obtained from our EXAFS, representing a 1.7% lattice contraction. It has been well documented that Au NCs normally showed lattice contraction (up to a few percent) relative to bulk Au.[36,37] The lattice contraction of metal NCs can be simply described with a liquid-drop model (to lower the surface energy).[38] Note that only a single Au–Au path was used in our EXAFS fit. Indeed, the structure of $Au_{25}(SR)_{18}$ reported by Murray *et al.*[3] shows three types of Au–Au bonds in the Au_{13} core, i.e., bonds between central Au and the shell surrounding it (average of 2.79 Å), bonds between the pair of core-atoms directly below the "staple" (average of 2.81 Å), and other core Au–Au bonds (average of 2.96 Å). In addition, possible aurophilic bonding (average of 3.16 Å) was also proposed. However, the range of EXAFS data (3–12 Å) used in the present work does not allow us to resolve these bonds whose lengths are only slightly different. More accurate bond distance results have to wait for higher quality EXAFS data with longer k-range [e.g., low temperature EXAFS (Ref. 36)].

B. Au L_3-edge XANES

A very useful feature of XAS is that the near-edge spectrum (XANES) can probe the electronic behavior of NCs.[22] In Fig. 4, the Au L_3-edge XANES of Au-BSA and bulk Au are presented. The small peak right after the edge jump is historically called white line.[22] The Au L_3-edge white line probes the electronic transition from 2p to unoccupied 5d states. A more intense white line corresponds to more unoccupied 5d states (d-hole) or less 5d-electrons. In Fig. 4, Au-BSA is found to have a more intense white line than the bulk. Based on the theoretical method developed by Sham *et al.*,[31] we semiquantitatively calculated the d-hole count change of the NCs relative to bulk Au, which yields an increase of 0.047 e^- in the d-hole counts. In other words, Au atoms in the NCs show an average d-electron depletion of 0.047 e^-. It should be noted that the d-hole information obtained here was based on the assumption of the statistical distribution of the $d_{5/2}$ and $d_{3/2}$ holes and hence is only semiquantitative. Therefore, the scale of this value (~0.05 e^-) would be more significant than the value itself. Nevertheless, it does provide useful data from the experimental perspective that can be compared with our theoretical results to be presented in the next section. In addition, it may serve as a reference for a more accurate investigation in the future. In Fig. 4 inset, a small positive shift (0.5 ± 0.1 eV) of the threshold energy E_0

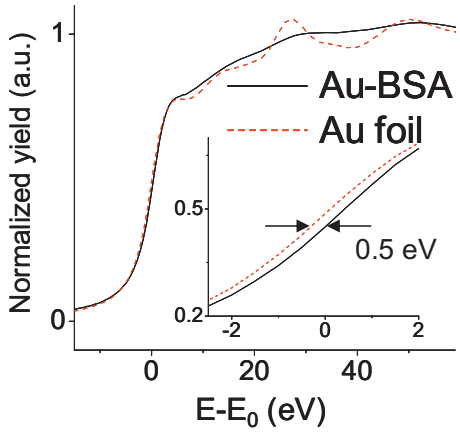

FIG. 4. Au L_3-edge XANES of Au-BSA (solid line) and Au foil (dashed line). A comparison of the edge shift between the two samples is shown in the inset.

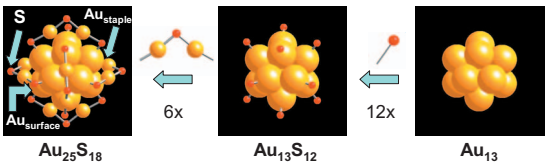

FIG. 5. A schematic illustration of the atomic structure of $Au_{25}S_{18}$, $Au_{13}S_{12}$, and Au_{13} clusters used for l-DOS calculations. In $Au_{25}S_{18}$, the Au atoms in the staples were deliberately made smaller to be distinguishable from the core Au atoms. The $Au_{surface}$ and Au_{staple} sites were also marked in the figure (the Au_{center} site is invisible).

was also observed by comparing the spectrum of Au-BSA with the simultaneously collected data of Au foil. The higher binding energy of Au-BSA is consistent with the result of its d-electron depletion from the white line calculation. The origin of d-electron depletion will be discussed in conjunction with the theoretical results in the next section.

C. L-DOS calculations

To obtain further insights into the effect of the "staple" motif on the electronic behavior of the Au NCs, l-DOS calculation of the $Au_{25}(SR)_{18}$ model cluster was conducted using *ab initio* FEFF8 program. L-DOS calculation using FEFF8 program has been proved in general to be comparable with modern band-structure methods.[26] Recently, Dimakis *et al.*[39] has further verified the reliability of FEFF8 based l-DOS calculation of Pt catalysts where relativistic effect is significant; that is, the electron density data calculated with FEFF8 program was consistent with the DFT results from Mulliken population analysis. In order to use FEFF8 based l-DOS calculation to systematically investigate effect of the "staple" motif on the electronic behavior of Au_{25}, two relevant model clusters, $Au_{13}S_{12}$ and Au_{13}, were also constructed. Atomic structures of the three model clusters are illustrated in Fig. 5. All the three model clusters have the same icosahedral Au_{13} core (i.e., same coordinates of the Au_{13} core for the l-DOS calculations). The $Au_{13}S_{12}$ model was constructed by adding 12 S to the on-top site of each surface Au of the Au_{13} core. The only difference between $Au_{13}S_{12}$ and $Au_{25}S_{18}$ is the presence of six S–Au–S units in the latter, each unit connecting two surface S in $Au_{13}S_{12}$ to form totally 6 –S–Au–S–Au–S– "staples." For convenience in the discussion, the three types of Au atoms in $Au_{25}S_{18}$ illustrated in Fig. 5 are referred to as Au_{center}, $Au_{surface}$, and Au_{staple}, respectively.

The site-specific electronic configuration of the three model clusters and bulk Au, together with the charge transfer (CT) information, are given in Table II. The CT data presented in the table include contributions of s, p and d-electrons and a positive CT number corresponds to a depletion of electrons. In general, the amount of CT is relatively small, consistent with the theoretical results obtained using other methods.[40] The $Au_{surface}$ atoms in bare Au_{13} cluster show a zero CT and increased d-electron count, which is expected. However, the Au_{center} atom exhibits an unexpected positive CT and a decreased d-electron count. We attribute this to the geometric effect of the model cluster in that the Au_{13} bare cluster was taken from the core of the $Au_{25}S_{18}$ model cluster, which is not perfectly symmetric (e.g., Au–Au bond length ranging from ~2.8 to ~2.9 Å for the Au_{13} core). Nevertheless, due to its very low fractional abundance (1/13 or 1/25), the influence of Au_{center} atom is far less significant than $Au_{surface}$ and Au_{staple} atoms. Both of the two thiolate clusters show an average CT of ca. 0.18 e^- (depletion of electrons), mainly due to the loss of electrons from Au to S atoms. Interestingly, presence of the "staple" motif causes the CT number of $Au_{surface}$ atoms in $Au_{25}S_{18}$ decrease (0.167 $e^- \rightarrow 0.097$ e^-) relative to their counterparts in $Au_{13}S_{12}$. In other words, the Au-thiolate "staples" make the Au–S bonds between $Au_{surface}$ and S atoms less polar than those in $Au_{13}S_{12}$. In addition, the Au_{staple} atom shows largest amount of CT (0.242 e^-) among the three sites in $Au_{25}S_{18}$. The fact that the average CT number of Au_{staple} is only 0.242 e^- indicates that Au–S bonds in the "staples" are essentially of covalent nature. This is somewhat surprising since Au-thiolate bonds in $(–Au–SR–)_n$ polymers are normally referred to as ionic bonds. However, this finding can still be understandable if one considers the fact that the electronegativity of Au (2.54) is very close to that of S (2.58). In addition, the proposed aurophilic interaction[3] between Au_{staple} and $Au_{surface}$ atoms in $Au_{25}S_{18}$ may also contribute to this. Overall, these results clearly indicate that the presence of the "staple" motif influences the electronic behavior of all the three types of Au atoms in $Au_{25}S_{18}$.

Effect of the "staple" motif on d- and s-electron behavior is particularly interesting in light of the "superatom" theory that accounts for the unusually high stability of Au_{25}.[40] To more clearly illustrate the d- and s-electron behavior of the model clusters, plots of Δd- and Δs-electron counts (change relative to that of the bulk) from each representative site are shown in Figs. 6 and 7, respectively. In Fig. 6, the experimental data of Δd-electron counts of Au-BSA is also presented for comparison purpose. The calculated Δd-electron counts of $Au_{25}S_{18}$(−0.050 e^-) is in good agreement of the experimentally determined data of Au-BSA (−0.047 e^-).

TABLE II. Electronic configuration and CT of each representative Au site of $Au_{25}S_{18}$, $Au_{13}S_{12}$, Au_{13}, and bulk Au obtained by FEFF8 l-DOS calculation.

	Au_{center}		$Au_{surface}$		Au_{staple}		Av
	Configuration	CT[a]	Configuration	CT[a]	Configuration	CT[a]	CT
$Au_{25}S_{18}$	$s^{0.806}$ $p^{0.686}$ $d^{9.317}$	0.191	$s^{0.847}$ $p^{0.687}$ $d^{9.359}$	0.097	$s^{0.917}$ $p^{0.707}$ $d^{9.279}$	0.242	0.170
$Au_{13}S_{12}$	$s^{0.795}$ $p^{0.753}$ $d^{9.149}$	0.305	$s^{0.884}$ $p^{0.593}$ $d^{9.356}$	0.167	⋯	⋯	0.178
Au_{13}	$s^{0.777}$ $p^{0.620}$ $d^{9.289}$	0.314	$s^{0.952}$ $p^{0.569}$ $d^{9.479}$	0	⋯	⋯	0.023
Bulk Au	$s^{0.855}$ $p^{0.775}$ $d^{9.369}$	0	⋯	⋯	⋯	⋯	0

[a]CT: Charge transfer (in unit of e^-).

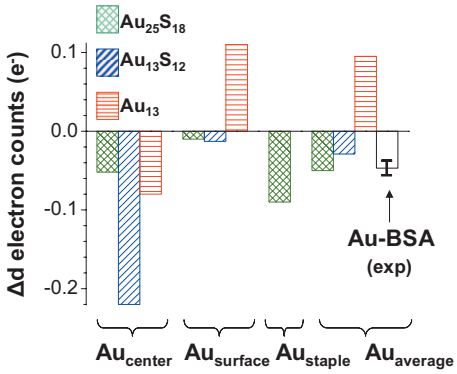

FIG. 6. A chart of Δd electron counts, i.e., d(NC)-d(bulk), of three model clusters at each specific site (Au_{center}, $Au_{surface}$, and Au_{staple}). The experimental data (with error bar) of Au-BSA is also presented for comparison.

This reassures the reliability of the FEFF8 based l-DOS calculation method used in the work. However, one should not take such an agreement as an absolute proof, particularly when considering the limited accuracy (semiquantitative) of the experimental d-hole data. In Fig. 6, we see that average d-electron counts of the two thiolate-Au clusters were both decreased relative to that of bulk Au (−0050 e^- for $Au_{25}S_{18}$ and −0.029 e^- for $Au_{13}S_{12}$), whereas that of the bare cluster Au_{13} show an increase by 0.095 e^-. The different d-electron behavior between the bare and thiolate-Au clusters in Fig. 6 is consistent with the experimental XANES results of Au NCs capped with weakly interacting amine and strongly binding thiolate ligands.[38] The increased d-electron counts of bare Au NCs (or NCs capped with weakly binding ligands) can be understood using the s-p-d hybridization model.[25] The narrowing of d-band in the NCs (due to a decreased CN) results in a less pronounced overlap between d- and s/p-bands. As a consequence, the amount of electrons flowing from d-band to s/p-band was decreased. The d-electron depletion of Au in the thiolate-Au NCs was mainly caused by the CT from Au to S due to the higher electronegativity of S than Au.[23] Note that although the Au_{center} atom in $Au_{13}S_{12}$ shows the largest amount of d-charge depletion (−0.220 e^-), the average d-electron behavior was not much influenced due to its very low fraction (1/13) relative to that of $Au_{surface}$ atoms (12/13). It is also clear in Fig. 6 that the overall d-electron depletion in $Au_{25}S_{18}$ is mainly determined by the decreased d-electron counts of Au_{staple} atoms (Δd =−0.090 e^-). These results, in association with the experimental data, consistently indicate that the d-electron depletion is of very small scale (<0.1 e^-) and it is mainly caused by the Au–S bonding effect associated with the "staple" motif in the Au NCs.

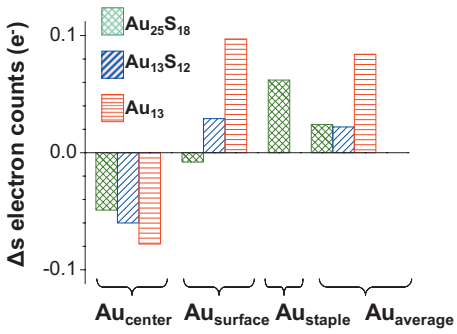

FIG. 7. A chart of Δs electron counts, i.e., s(NC)-s(bulk), of three model clusters at each specific site (Au_{center}, $Au_{surface}$, and Au_{staple}).

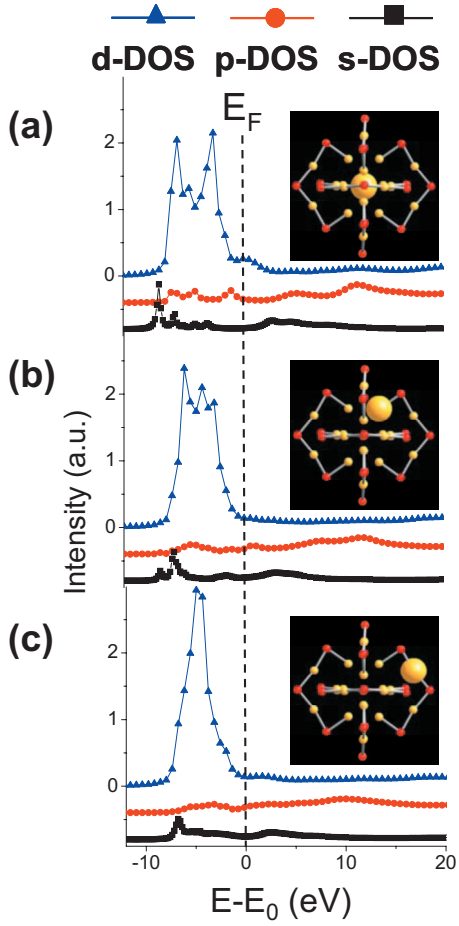

FIG. 8. FEFF8 calculated s (square), p (circle), and d (triangle) bands of $Au_{25}S_{18}$ from a site-specific perspective. Each Au site was also schematically illustrated in the figure. The Fermi level (E_F) was all aligned to E=0 eV.

In Fig. 7, the average s-electron counts of all the three clusters were found to increase relative to that of the bulk. The Au_{13} cluster shows the largest amount of increased Δs-electron counts (0.084 e^-). The two thiolate-Au clusters show very similar average Δs-electron counts (0.024 e^- for $Au_{25}S_{18}$ and 0.022 e^- for $Au_{13}S_{12}$), both lower than that of the bare cluster. A close inspection of the site-specific Δs-electron data of the two thiolate-Au clusters in Fig. 7 indicates that the s-electron behavior of these two clusters is quite different. In the absence of the "staple" motif, the $Au_{surface}$ atom in $Au_{13}S_{12}$ gains s-electron (0.029 e^-) relative to the bulk. In contrast, the $Au_{surface}$ atom in $Au_{25}S_{18}$ slightly losses some s-electron (−0.008 e^-). In other words, presence of the "staple" motif causes a net change of s-electron of 0.037 e^- for the $Au_{surface}$ atom when going from $Au_{13}S_{12}$ to $Au_{25}S_{18}$. In addition, Au_{staple} atoms in $Au_{25}S_{18}$ were found to gain s-electron by 0.062 e^- relative to the bulk. Such a gain of s-electron compensates the depletion of s-electron at Au_{center} and $Au_{surface}$ sites, giving an overall increase of s-electron by 0.024 e^- per Au atom.

Figure 8 shows the FEFF8 calculated s, p, and d bands of

each Au atomic site (i.e., Au_{center}, $Au_{surface}$, and Au_{staple}) in $Au_{25}S_{18}$. The most interesting observation is the difference of d-band shape. As shown in Figs. 8(a)–8(c), the d bands become narrower when going from Au_{center} to $Au_{surface}$ and then to Au_{staple}. In addition, the top of the d bands moves away systematically from the Fermi level as the bands become narrower. Narrowing of the d bands indicate that d-electrons become more localized in the order of $Au_{center} \rightarrow Au_{surface} \rightarrow Au_{staple}$. The fact that d-band of Au_{staple} is very sharp implies that Au atoms in the "staples" show moleculelike electronic behavior.

It is worthwhile to correlate our l-DOS results with some of the recent findings in the studies of Au-thiolate nanostructures in the context of Au-thiolate "staple" motif. Park and Palmer[41] reported a striking free-electronlike electronic behavior of Au (111) surface caused by the formation of Au-thiolate monolayer. Note that for bare Au surface, the 6s electrons are screened quite strongly by the 5d band, thus exhibiting a damping of the Au plasmon (i.e., less free-electronlike behavior). Park and Palmer[41] attributed the enhanced free-electronlike behavior of thiolate-covered Au surface to the weakened screening of Au 6s electrons by the 5d band. They also used the "superatom" theory for Au-thiolate NCs (Ref. 40) to qualitatively interpret their experimental results.[41] Our experimental and theoretical results are not only consistent with the experimental data of Park and Palmer[41] but offer a more detailed interpretation to their findings. Specifically, our l-DOS calculations show that Au_{staple} and $Au_{surface}$ atoms gain 6s electron and lose 5d electron (accompanied by 5d band narrowing) at the Au-thiolate interface. This will cause the Au 6s electrons less screened than those in the bare surface (due to both an increase of 6s-electron count and a weakened screening by the narrowed and electron-depleted 5d band). As a result, the 6s electrons show a more free-electronlike behavior. Although our l-DOS calculation was based on the "staple" motif in Au_{25} NCs, recent X-ray diffraction studies did show evidence of the presence of –S–Au–S– "staples" in thiol monolayer covered Au (111) surface.[7]

The "superatom" theory has been used successfully to account for the unusually high stability of $Au_{25}(SR)_{18}$ cluster.[40] According to this theory, the delocalized "superatomic orbitals" of metal clusters consist of $1S^2 1P^6 1D^{10} 2S^2 1F^{14} 2P^6 1G^{18} 2D^{10}, \ldots$, where S-P-D-F-G refers to the angular momentum character. In the case of Au NCs, the delocalized "superatomic orbitals" are mainly originated from the atomic 6s orbitals (i.e., each Au atom contributing one 6s electron). In $Au_{25}(SR)_{18}$ an eight-electron ($1S^2 1P^6$) shell closing was achieved when each of the 13 Au atoms in the icosahedral core donates one s-electron to delocalized orbitals and each of the six –S–Au–S–Au–S– "staples" formally takes one electron into a localized orbital. By including one extra electron from the anionic $Au_{25}(SR)_{18}^-$ into the delocalized orbitals, there are totally $1+(13-6)=8$ delocalized electrons forming the closed shell in the highly stable "superatom" (an analog to the noble gas). Our l-DOS results indicate that presence of the Au-thiolate "staples" causes a very small change to the s-electron counts of each Au site in the cluster (an increase of <0.1 electron per atom relative to that of bulk Au), supporting the "superatom" theory. In addition, results of the d-band shape of the three sites in $Au_{25}S_{18}$ shown in Fig. 8 coincide with the "superatom" shell closing theory; that is, the Au_{13} core is somewhat metallic whereas Au_{staple} atoms show moleculelike behavior.

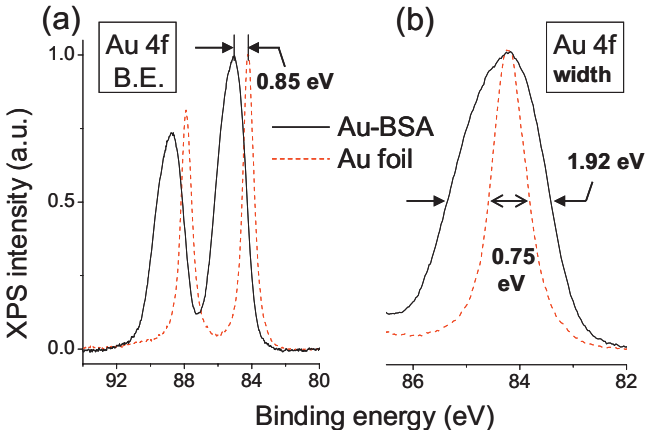

FIG. 9. Au 4f XPS spectra of Au-BSA and Au foil. The XPS intensity was normalized to 1 for comparison purpose. (a) original XPS data showing the 4f binding energy shift; and (b) horizontally shifted spectra illustrating the difference of the spectral shape.

D. Au 4f XPS results

In Fig. 9, we present the Au 4f core-level XES data of Au-BSA and bulk Au. In Fig. 9(a), the binding energy of Au 4f peak of Au-BSA shifts by 0.85 ± 0.10 eV toward higher energy (relative to the bulk). Negishi *et al.*[42] has compared the Au 4f cove-level binding energy of a series of thiolate-protected Au NCs ($Au_{10}-Au_{39}$). The XPS results of Negishi *et al.*[42] showed a positive shift of 0.8–0.9 eV for their Au_{25} NCs. The 0.85 eV shift observed in Fig. 9(a) is in good agreement with Negishi's results. Moreover, the calculated d-DOS results and XANES data can provide a reliable interpretation on the origin of the positive Au 4f binding energy shift for Au-BSA. It has been generally proposed that two mechanisms are responsible for the core-level binding energy shift of transition metal NCs.[43] The first mechanism is the initial-state effect, which is due to the changed electronic configuration of metal atoms in the NCs.[28] The second one is known as final-state effect, which was based on the Coulomb charging effect associated with small metal clusters due to their reduced conductivity.[29] As is well known, the white line in XANES is mainly associated with the initial effect.[44] Recalling that a 0.5 eV positive shift was found for Au-BSA from the XANES in Fig. 4, the observed 0.85 eV XPS core-level binding energy shift is well correlated with the XANES E_0 shift. The positive 4f binding energy shift for the NCs should be largely associated with the initial state effect and correlate well with the result of d-electron depletion obtained in the Au L_3-edge XANES analysis. However, contribution of the final-state effect cannot be completely ruled out. In addition, we note that the comparison of deep $2p_{3/2}$ core-level threshold (i.e., E_0 at Au L_3-edge) with the shallow Au 4f level is not as good as the comparison between two simi-

larly deep core levels. This should also contribute to the difference of the energy shifts between the XANES and XPS data.

In Fig. 9(b), we compare the shape of Au 4f bands of Au-BSA and the bulk. Significant 4f line-broadening was found for Au-BSA relative to Au foil (1.92 eV versus 0.75 eV). In addition, the 4f line-broadening is found to be asymmetric, the higher binding energy side being broadened more significantly. It has been known that the XPS Au 4f component from Au–S bonds in thiolate-capped Au nanoparticles is positively shifted relative to that from Au–Au bonds.[23] Similarly, the observed asymmetric broadening at higher binding energy side in Fig. 9(b) should be related to the significant contribution of Au–S bonds to the Au 4f peak. Indeed, due to the unique staplelike structure in $Au_{25}(SR)_{18}$, nearly all the Au atoms (24 of 25) are bound to S atoms.[23] Moreover, presence of the giant protecting ligands (BSA) may lead to Coulomb charging effect, which also possibly contributes to the observed line-broadening of Au 4f peak.

IV. CONCLUDING REMARKS

We have used experimental x-ray spectroscopy techniques and theoretical l-DOS calculations to study the structure and electronic behavior of BSA-encapsulated Au NCs and $Au_{25}(SR)_{18}$ model cluster. Important findings in this work consist of: (i) structural analysis of protein/thiolate-protected Au NCs with "staple" motif conducted by EXAFS for the first time, (ii) electronic properties of Au-BSA NCs experimentally illustrated using XANES and XPS, and (iii) a detailed picture of the electronic behavior of the NCs revealed by theoretical l-DOS studies. These findings will be useful to more thoroughly understand the structure-property relationship of Au-thiolate NCs with "staple" motif. The experimental and theoretical techniques used here are promising in the structural and electronic studies of other Au-thiolate NCs [e.g., Au_{20} (Ref. 6) and Au_{38} (Ref. 14)] whose total structures have not been determined.

Finally, we would like to comment on the limitations and advantages of using XAS and associated techniques in the studies of Au-thiolate NCs with "staple" motif, which is a recently emerged fascinating area that stimulates extensive research interests. Although XAS (i.e., the EXAFS part) is widely considered as a local structure characterization tool complementary to the single crystal diffraction technique, if single crystals are available, XAS cannot compete with the diffraction technique in determining the total structure of materials. Indeed, only single crystal diffraction measurement will allow one to accurately determine the total structure of thiolate-protected Au NCs (e.g., Au_{102} and Au_{25}). In comparison, XAS can just provide a one-dimensional picture of atomic structure by analysis of the CN and bond distance. Nevertheless, there are a few important advantages of using XAS in the studies of these thiolate-Au NCs. First, no single crystals are needed in the EXAFS structural analysis. This may be particularly useful for the study of NCs whose single crystals cannot be obtained.[20] Second, in addition to local structural studies, XAS can simultaneously provide valuable information about the electronic properties of Au atoms. Joint use of experimental and theoretical l-DOS results can provide a detailed picture of the s, p, d-electron behavior from a site-specific perspective. Third, XAS will potentially allow one to conduct *in situ* liquid-phase experiments to follow the evolution of structural and electronic properties of Au NCs during the course of chemical reactions [e.g., oxidation of anionic Au_{25}^- to neutral Au_{25} (Ref. 13)]. We are in the process of using the *in situ* XAS technique in such studies.

ACKNOWLEDGMENTS

The research in this work is supported by Dalhousie University and NSERC Canada. The infrastructure of laboratory research facilities are supported by CFI. The Canadian light source (CLS) is supported by NSERC, CIHR, NRC, and the University of Saskatchewan. We acknowledge the CLS staff scientist Dr. Ning Chen (HXMA beamline), Dr. Robert Blyth (SGM beamline) and Dr. Tom Reigers (SGM beamline) for the synchrotron technical support. We also thank Dr. Rongchao Jin (Carnegie Mellon University) for providing insightful comments on this work.

[1] P. D. Jadzinsky, G. Calero, C. J. Ackerson, D. A. Bushnell, and R. D. Kornberg, Science **318**, 430 (2007); R. L. Whetten and R. C. Price, *ibid.* **318**, 407 (2007); P. Ball, Nature Mater. **6**, 927 (2007).
[2] A. W. Castleman and S. N. Khanna, J. Phys. Chem. C **113**, 2664 (2009).
[3] M. W. Heaven, A. Dass, P. S. White, K. M. Holt, and R. W. Murray, J. Am. Chem. Soc. **130**, 3754 (2008).
[4] J. Akola, M. Walter, R. L. Whetten, H. Hakkinen, and H. Gronbeck, J. Am. Chem. Soc. **130**, 3756 (2008).
[5] M. Zhu, E. Lanni, N. Garg, M. E. Bier, and R. Jin, J. Am. Chem. Soc. **130**, 1138 (2008).
[6] M. Z. Zhu, H. F. Qian, and R. C. Jin, J. Am. Chem. Soc. **131**, 7220 (2009).
[7] A. Cossaro, R. Mazzarello, R. Rousseau, L. Casalis, A. Verdini, A. Kohlmeyer, L. Floreano, S. Scandolo, A. Morgante, M. L. Klein, and G. Scoles, Science **321**, 943 (2008).
[8] H. Häkkinen, Chem. Soc. Rev. **37**, 1847 (2008).
[9] Y. Pei, Y. Gao, and X. C. Zeng, J. Am. Chem. Soc. **130**, 7830 (2008).
[10] Y. Gao, N. Shao, and X. C. Zeng, ACS Nano **2**, 1497 (2008); Y. Li, G. Galli, and F. Gygi, *ibid.* **2**, 1896 (2008).
[11] O. Lopez-Acevedo, J. Akola, R. L. Whetten, H. Gronbeck, and H. Hakkinen, J. Phys. Chem. C **113**, 5035 (2009).
[12] R. L. Whetten, J. T. Khoury, M. M. Alvarez, S. Murthy, I. Vezmar, Z. L. Wang, P. W. Stephens, C. L. Cleveland, W. D. Luedtke, and U. Landman, Adv. Mater. **8**, 428 (1996); A. C. Templeton, M. P. Wuelfing, and R. W. Murray, Acc. Chem. Res. **33**, 27 (2000); M. C. Daniel and D. Astruc, Chem. Rev. (Washington, D.C.) **104**, 293 (2004); R. W. Murray, *ibid.* **108**, 2688 (2008); N. K. Chaki, Y. Negishi, H. Tsunoyama, Y. Shichibu, and T. Tsukuda, J. Am. Chem. Soc. **130**, 8608 (2008); Z. Wu, J. Suhan, and R. C. Jin, J. Mater. Chem. **19**, 622 (2009).
[13] M. Z. Zhu, W. T. Eckenhoff, T. Pintauer, and R. C. Jin, J. Phys. Chem. C **112**, 14221 (2008).
[14] H. F. Qian, M. Z. Zhu, U. N. Andersen, and R. C. Jin, J. Phys. Chem. A **113**, 4281 (2009).
[15] O. Toikkanen, V. Ruiz, G. Ronholm, N. Kalkkinen, P. Liljeroth, and B. M. Quinn, J. Am. Chem. Soc. **130**, 11049 (2008).
[16] J. P. Xie, Y. G. Zheng, and J. Y. Ying, J. Am. Chem. Soc. **131**, 888 (2009).
[17] S. J. L. Billinge and I. Levin, Science **316**, 561 (2007).
[18] A. Dass, K. Holt, J. F. Parker, S. W. Feldberg, and R. W. Murray, J. Phys. Chem. C **112**, 20276 (2008); A. Dass, G. R. Dubay, C. A. Fields-Zinna, and R. W. Murray, Anal. Chem. **80**, 6845 (2008).
[19] S. A. Miller, J. M. Womick, J. F. Parker, R. W. Murray, and A. M. Moran, J. Phys. Chem. C **113**, 9440 (2009).
[20] Z. W. Wu, C. Gayathri, R. R. Gil, and R. C. Jin, J. Am. Chem. Soc. **131**, 6535 (2009).
[21] G. H. Via, J. H. Sinfelt, and F. W. Lytle, J. Chem. Phys. **71**, 690 (1979);

A. I. Frenkel, C. W. Hills, and R. G. Nuzzo, J. Phys. Chem. B **105**, 12689 (2001); J. Zhang, K. Sasaki, E. Sutter, and R. R. Adzic, Science **315**, 220 (2007).
[22] J. H. Sinfelt and G. D. Meitzner, Acc. Chem. Res. **26**, 1 (1993).
[23] P. Zhang and T. K. Sham, Phys. Rev. Lett. **90**, 245502 (2003).
[24] A. L. Ankudinov, J. J. Rehr, J. J. Low, and S. R. Bare, J. Chem. Phys. **116**, 1911 (2002); J. D. Grunwaldt, M. Caravati, and A. Baiker, J. Phys. Chem. B **110**, 9916 (2006).
[25] F. Liu, D. Wechsler, and P. Zhang, Chem. Phys. Lett. **461**, 254 (2008).
[26] A. L. Ankudinov, B. Ravel, J. J. Rehr, and S. D. Conradson, Phys. Rev. B **58**, 7565 (1998).
[27] M. G. Mason, L. J. Gerenser, and S. T. Lee, Phys. Rev. Lett. **39**, 288 (1977); C. Kuhrt and M. Harsdorff, Surf. Sci. **245**, 173 (1991); I. Coulthard, S. Degen, Y. J. Zhu, and T. K. Sham, Can. J. Chem. **76**, 1707 (1998); G. A. Somorjai, R. L. York, D. Butcher, and J. Y. Park, Phys. Chem. Chem. Phys. **9**, 3500 (2007); T. K. Sham, P. S. G. Kim, and P. Zhang, Solid State Commun. **138**, 553 (2006).
[28] M. G. Mason, Phys. Rev. B **27**, 748 (1983).
[29] G. K. Wertheim, S. B. Dicenzo, and S. E. Youngquist, Phys. Rev. Lett. **51**, 2310 (1983).
[30] T. Ressler, J. Synchrotron Radiat. **5**, 118 (1998).
[31] I. Coulthard and T. K. Sham, Phys. Rev. Lett. **77**, 4824 (1996).
[32] C. M. Aikens, J. Phys. Chem. C **112**, 19797 (2008).
[33] L. D. Menard, H. P. Xu, S. P. Gao, R. D. Twesten, A. S. Harper, Y. Song, G. L. Wang, A. D. Douglas, J. C. Yang, A. I. Frenkel, R. W. Murray, and R. G. Nuzzo, J. Phys. Chem. B **110**, 14564 (2006).
[34] J. L. Burt, C. Gutierrez-Wing, M. Miki-Yoshida, and M. Jose-Yacaman, Langmuir **20**, 11778 (2004).
[35] Y. Shichibu, Y. Negishi, H. Tsunoyama, M. Kanehara, T. Teranishi, and T. Tsukuda, Small **3**, 835 (2007).
[36] D. Zanchet, H. Tolentino, M. C. M. Alves, O. L. Alves, and D. Ugarte, Chem. Phys. Lett. **323**, 167 (2000).
[37] W. J. Huang, R. Sun, J. Tao, L. D. Menard, R. G. Nuzzo, and J. M. Zuo, Nature Mater. **7**, 308 (2008).
[38] P. Zhang and T. K. Sham, Appl. Phys. Lett. **81**, 736 (2002).
[39] N. Dimakis, H. Iddir, R. R. Diaz-Morales, R. X. Liu, G. Bunker, E. H. Chung, and E. S. Smotkin, J. Phys. Chem. B **109**, 1839 (2005).
[40] M. Walter, J. Akola, O. Lopez-Acevedo, P. D. Jadzinsky, G. Calero, C. J. Ackerson, R. L. Whetten, H. Gronbeck, and H. Hakkinen, Proc. Natl. Acad. Sci. U.S.A. **105**, 9157 (2008).
[41] S. J. Park and R. E. Palmer, Phys. Rev. Lett. **102**, 216805 (2009).
[42] Y. Negishi, K. Nobusada, and T. Tsukuda, J. Am. Chem. Soc. **127**, 5261 (2005).
[43] G. K. Wertheim, Z. Phys. D: At., Mol. Clusters **12**, 319 (1989).
[44] M. Cini, M. Decrescenzi, F. Patella, N. Motta, M. Sastry, F. Rochet, R. Pasquali, A. Balzarotti, and C. Verdozzi, Phys. Rev. B **41**, 5685 (1990).